PROCEEDINGS OF SPIE

SPIEDigitalLibrary.org/conference-proceedings-of-spie

Time-dependence of the transmission matrix of a specialty few-mode fiber

J. Yammine, A. Tandjè, Michel Dossou, L. Bigot, E. R. Andresen

J. Yammine, A. Tandjè, Michel Dossou, L. Bigot, E. R. Andresen, "Time-dependence of the transmission matrix of a specialty few-mode fiber," Proc. SPIE 10947, Next-Generation Optical Communication: Components, Sub-Systems, and Systems VIII, 1094702 (1 February 2019); doi: 10.1117/12.2508301

SPIE.

Event: SPIE OPTO, 2019, San Francisco, California, United States

Time-dependence of the transmission matrix of a specialty few-mode fiber.

J. Yammine[1], A.Tandjè[1, 2], Michel Dossou[2], L. Bigot[1], and E. R. Andresen[1,a)]
[1)]Univ. Lille, CNRS, UMR 8523 - PhLAM - Physique des Lasers Atomes et Molécules, F-59000 Lille, France.
[2)] Ecole Polytechnique d'Abomey-Calavi (EPAC), Univ. D'Abomey-Calavi (UAC), Cotonou, Bénin.

ABSTRACT

We report on the time-resolved measurement of the full transmission matrix (TM) of a short length of specialty annular-core few-mode fiber which guides 10 vector modes. We show how our method can isolate the fiber TM from "misalignment" contributions from free space optics upstream and downstream of the fiber. From measurements spanning two days, we extract the drift of the fiber TM. We show that drifts in the TM elements are mostly described as correlated phase variations rather than amplitude variations. We show that an empirical model of the fiber TM parametrized in one parameter can successfully account for the drift.
Keywords: Ring-core fiber, OAM mode, Multi-modal channel, Modal division multiplexing, Space-division multiplexing, Fiber optic communications.

1. INTRODUCTION

The World's communication networks based on single-mode fiber (SMF) are currently approaching their capacity limits [1]. These limits can be repelled by using spatial division multiplexing (SDM) based on multi-core fibers (MCF) or mode division multiplexing (MDM) based on few-mode fibers (FMF) [2-4]. A MCF with N cores could then be compared to N independent SMFs, each core acting as an independent pathway. Nevertheless, except for very short links, the interaction between cores leads to an energy transfer that appears as a limitation. This interaction, also known as inter-core cross-talk, is governed by the coupled-mode theory [5], so the cross-talk is a function of, among others, the effective index differences between the cores which, in turn, are sensitive to strain, temperature, etc. which must be expected to vary both as a function of distance and time. Diverse papers have described the time evolution of transmission quality in MCF [6-14]. A variation of inter-core cross-talk that can reach 10 dB has been shown by experimental measurements [6-10,12]. The reason why the knowledge of the inter-core cross-talk variability is a must is due to its important consequences on MCF network design with optimized performance in all conditions. In order to assist in designing MCF networks, channel models for MCFs have been suggested [11,13,14].
For FMFs, these same issues are expected to be found. However, to the best of our knowledge, the temporal behavior of the FMF optical channel has not been investigated as for their MCF counterparts. Regarding the time behavior of FMFs, it is essential to know the time evolution of the cross-talk between degenerate modes within a mode family (a mode family being a group of modes whose effective indices are very close), as well as the cross-talk between any two groups of modes. However, the access to each independent FMF modes, acting as individual spatial channels is a difficult question. In practice, the use of FMFs needs the presence of modal multiplexers or demultiplexers, which can add non-negligible cross-talk, either intrinsic, or as a result of misalignment. These accumulated cross-talk contributions are hard to discriminate. Here, we present a method for isolating the transmission matrix (TM) of the FMF -the "fiber TM"- from the interfacing components. We use this to perform time-resolved measurements of the TM of a specialty, annular-core fiber supporting 10 vector modes and thus evaluate the temporal behavior of the optical channel.

Next-Generation Optical Communication: Components, Sub-Systems, and Systems VIII,
edited by Guifang Li, Xiang Zhou, Proc. of SPIE Vol. 10947, 1094702 · © 2019 SPIE
CCC code: 0277-786X/19/$18 · doi: 10.1117/12.2508301

2. EXPERIMENTAL

Annular-core fiber

For this study, we used an annular-core fiber fabricated at the FiberTech Lille platform (http://fibertech.univ-lille.fr/). Fig. 1(a) shows its measured refractive index profile. A scanning electron micrograph of the same fiber is presented in Fig. 1(b). Such a fiber is quite similar to that used by Bozinovic et al. to demonstrate Terabit-scale orbital angular momentum mode division multiplexing [15]. Its length was 1.5 m.

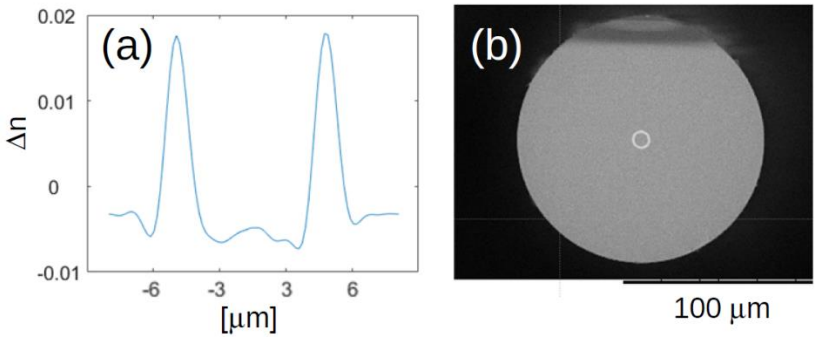

Figure 1. (a) Measured refractive index profile of the annular-core fiber as a function of the transverse coordinate. (b) Scanning electron micrograph of the fiber.

The experimental refractive index profile was used to model the fiber allowing us to predict the presence of 10 guided vector modes which are listed in Tab. 1 together with their calculated effective indices. From the calculated fields of the vector modes, we established a basis of linearly polarized modes with helical phase (see Tab. 2) which will be employed in the fiber TM measurement described below.

Table 1. Margins and print area specifications.

$Mode$	n_{eff}
$HE_{11}^{(e)}, HE_{11}^{(o)}$	1.4484829
TE_{01}	1.4471994
$HE_{21}^{(e)}, HE_{21}^{(o)}$	1.4471433
TM_{01}	1.4470770
$HE_{31}^{(e)}, HE_{31}^{(o)}$	1.4442856
$EH_{11}^{(e)}, EH_{11}^{(o)}$	1.4442890

Table 2. The linearly polarized, helical-phase mode basis.

#	(l, pol)	$Constituent\ vector\ modes$
1	$(0, h)$	$HE_{11}^{(e)}$
2	$(0, v)$	$HE_{11}^{(o)}$
3	$(-1, h)$	$(TE_{01} - jTM_{01}) + (HE_{21}^{(e)} - jHE_{21}^{(o)})$
4	$(1, h)$	$(HE_{21}^{(e)} + jHE_{21}^{(o)}) + (TE_{01} + jTM_{01})$
5	$(-1, v)$	$(HE_{21}^{(e)} + jHE_{21}^{(o)}) - (TE_{01} + jTM_{01})$
6	$(1, v)$	$(TE_{01} - jTM_{01}) - (HE_{21}^{(e)} - jHE_{21}^{(o)})$
7	$(-2, h)$	$(EH_{11}^{(e)} - jEH_{11}^{(o)}) + (HE_{31}^{(e)} - jHE_{31}^{(o)})$
8	$(2, h)$	$(HE_{31}^{(e)} + jHE_{31}^{(o)}) + (EH_{11}^{(e)} + jEH_{11}^{(o)})$
9	$(-2, v)$	$(HE_{31}^{(e)} + jHE_{31}^{(o)}) - (EH_{11}^{(e)} + jEH_{11}^{(o)})$
10	$(2, v)$	$(EH_{11}^{(e)} - jEH_{11}^{(o)}) - (HE_{31}^{(e)} - jHE_{31}^{(o)})$

The modes are denoted as (l, pol) where l represents the topological charge (i.e. the number of 2π phase turns per period) and pol is the polarization v or h. Our choice of mode basis was supported by the fact that the measurement was done in this basis and does not affect the result. Indeed, once established, the measured fiber TMs can be transformed into any other basis.

Transmission matrix measurement

The evolution of the electric fields going into and out of any type of fiber are described by the fiber TM. The TM provides a complete three-dimensional description of the linear behavior of the fiber, the input modes being the first dimension, the output modes presenting the second dimension and the wavelength being the third one. In our study, we chose to study the fiber TM for a single wavelength: this TM will describe the complete linear behavior of the fiber at this specific wavelength. The fiber TM measurement methodology used here is similar to the ones employed in Refs. [16] and [17]. The setup is presented in Fig. 2(a). We use a coherent laser source with a wavelength of 1550 nm (Yenista Tunics T100S). Using a polarization maintaining fiber optic coupler (not shown in Fig. 2(a)), the laser beam is then divided into two different beams, a signal beam and a reference beam. The signal beam is collimated, travels through a polarizing beam splitter (PBS) to reach the screen of a two-dimensional spatial light modulator (SLM, Meadowlark P1920-1625-HDMI). The polarization axis of the signal fiber, the PBS axis and the SLM axis are all parallel. A saw tooth phase mask with specific vertical and horizontal periodicity are displayed on the SLM, which will act as a diffraction grating, localizing the spot beam at a defined position with a desired angle. This method is used to scan the input end face with the focused signal beam: we can hence cover a large range of possible injection positions into the fiber. Each different angle is considered as a localized input mode. A half-wave plate (HWP) is inserted between the fiber and the SLM so we can control the polarization state of the injection beam, either vertical or horizontal state. The numerical aperture of the injection lens (0.5) is higher than the numerical aperture of the fiber (0.24), ensuring input localized modes sufficiently small to resolve the spatial structure of the fiber modes. The beam then travels through the fiber, emerges, is collimated, travels through another HWP and a PBS: the HWP will convert the polarization of the emerging beam into a linear polarization, whose axis is aligned with the PBS axis. The signal finally reaches a non-polarizing beam splitter (BS). The reference beam, on the other output fiber of the fiber optic coupler, travels an approximately equal optic path as the signal beam, while passing through an HWP and a PBS with the same polarization axis direction as the HWP and the PBS of the emerging signal fiber, and reaches the last BS. The two beams end their path on the sensor of an InGaAs camera (CAM), with a slight difference of the angle between them, enabling off axis holographic recording [16-18]. The combination of the two beams on the camera creates an interference pattern, which is saved for each localized input mode.

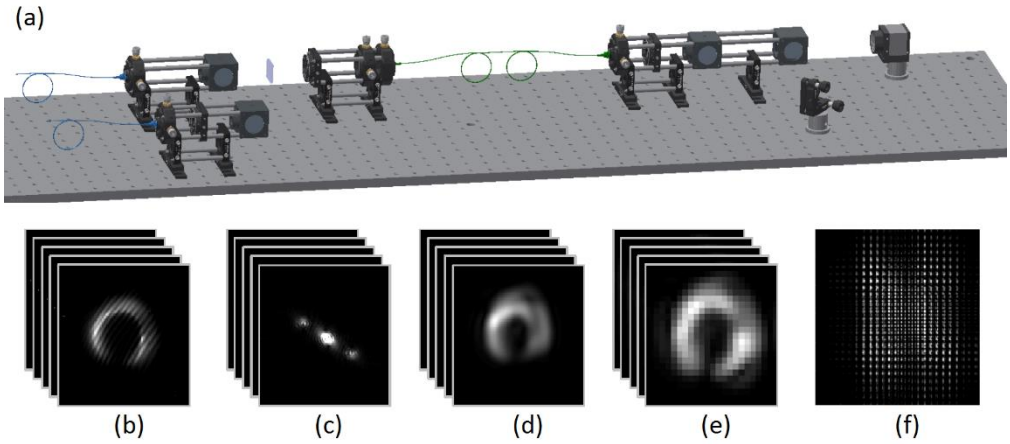

Figure 2. (a) Experimental setup. PM, polarization-maintaining; PBS, polarizing beam splitter; SLM, two-dimensional spatial light modulator; HWP, half-wave plate; BS, non-polarizing beam splitter; CAM, camera. Description of the data treatment: (b) Stack of interference images for 1 polarization combination. (c) Fourier transformation of the stack. (d) Inverse Fourier transformation of the filtered stack. (e) Down sampling of the images. (f) The transmission matrix of the stack. Only the norm of the complex-valued matrices is shown.

Once all four stacks are acquired, we begin the data analysis: each stack is analyzed on its own in the first step [Fig. 2(b)]. We apply a two-dimensional Fourier transformation to each image of the stack. The result is a stack of images with three peaks in the Fourier domain [Fig. 2(c)]. These images are then filtered in order to isolate one first-order peak. We apply an inverse Fourier transformation to recover a stack of the electric field of the signal beam on the CAM [Fig. 2(d)]. The phase drifts can be numerically subtracted from the stack of the electric field images of the reference localized input mode. Our CAM has a 320x256 resolution, so we chose to reduce the resolution of the images to 25x25, matching the number of elements in an image to the number of images in the stack [Fig. 2(e)]. The new stack of the down-sampled images is reshaped into a two-dimensional complex matrix: the rows of this matrix will contain all the localized input modes, and the columns will represent the localized output modes [Fig. 2(f)].
Such a matrix is obtained for every polarization combination possible (i.e. for each stack). The four obtained matrices are then combined to form the total system TM, which links all the input and all the output localized modes and their polarization states. This system TM, presented in Fig. 3, contains a contribution from the fiber itself (the fiber TM) as well as the "misalignment" contributions from the free-space optics between the SLM and the fiber; and between fiber and camera: we will seek to extract the fiber TM from this system TM. To this end we perform a singular value decomposition of the system TM and retain only the 10 first singular vectors (the first 10, corresponding to the number of guided modes, have singular values significantly larger than the rest).

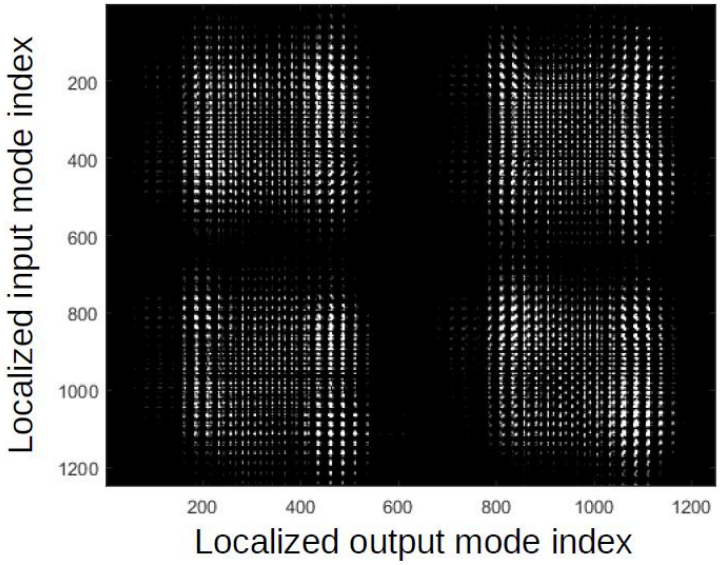

Figure 3. The total system TM. Only the norm of the complex valued matrix is displayed.

An iterative optimization algorithm is used to quantify the misalignment contribution: in each iteration the algorithm makes a guess for the misalignment, modifies the basis of the calculated modes by taking this misalignment into account, and then compares the mode space spanned by the modified calculated modes to the mode space spanned by the retained singular vectors. The algorithm continues to iterate and optimize its guess for the misalignment until it converges on maximum likeness between the two mode spaces. The misalignment can finally be removed from the system TM numerically, and a basis change is performed to express it in the basis of the calculated fiber modes. This is the TM of the fiber alone - the fiber TM - and we insist on the fact that our method is capable of isolating the contribution of the fiber from misalignment contributions like slow mechanical drift which can lead to contributions that would otherwise be interpreted as stemming from the fiber. With the current setup the measurement of the entire TM takes around 40 minutes when a basis of 25x25 localized modes is used. We measured a stack of fiber TMs over a time span of 36 h with the smallest time interval between subsequent measurements being about 2 h. The measurements were performed on an unconstrained fiber lying on an optical table in a half-turn shape in a laboratory room equipped with a standard air-conditioning unit, but no other special environmental control measures were taken. The temperature in the vicinity (few cm) of the fiber was logged every second.

3. RESULTS

Temporal evolution of the fiber TM

We acquired a stack of 11 fiber TMs over a time span of 36 h. The stack is indexed as follows

$$H_{kl}(t_i) \tag{1}$$

where k is the index of the input mode, l the index of the output mode, and i the temporal index. Fig. 4 shows one of these complex-valued fiber TMs. As expected, the matrix elements of significant amplitude are found in three blocks of size 2x2, 4x4, and 4x4 on the diagonal constituted by the three mode families with |l| = 0, 1, and 2 (cf Tab. 2), or in terms of the vector modes ($HE_{11}^{(e)}$, $HE_{11}^{(o)}$);(TE_{01}, $HE_{21}^{(e)}$, $HE_{11}^{(o)}$, TM_{01}); and ($HE_{31}^{(e)}$, $HE_{31}^{(o)}$, $EH_{11}^{(e)}$, $EH_{11}^{(o)}$).

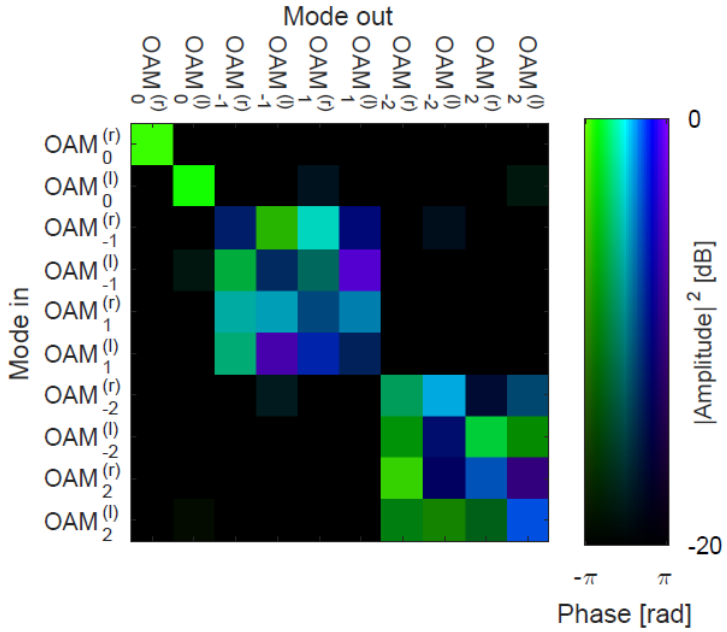

Figure 4. One example extracted from the stack of 11 measured fiber TMs. Notation of the modes as in Table 2. Note the doubly-graduated color map where color codes for the phase and the saturation codes for the norm-squared amplitude of the complex-valued fiber TM.

The small effective index differences within a family allow its members to couple freely in the presence of small perturbations of the fiber, while the large effective index differences between different groups of modes (> 10^{-3} cf Tab. 1) impede coupling (For reference, polarization- maintaining fibers typically have 10^{-4} index difference between the fast and slow polarization axes). We start the investigation of the temporal evolution of the fiber TM by examining the amplitudes and the phases of the elements of the fiber TMs. Figure 5(a) presents the temporal variation of the normalized amplitude defined as:

$$\Delta|H_{kl}|(t_i) = \frac{|H_{kl}(t_i)| - \langle|H_{kl}(t_i)|\rangle_i}{\langle|H_{kl}(t_i)|\rangle_i} \tag{2}$$

which describes the fractional amplitude variation from its mean calculated from the average over the time index i. Fig. 5(b) presents the temporal variation of the phase defined as:

$$\Delta\mathrm{Arg}[H_{kl}(t_i)] = \mathrm{Arg}[H_{kl}(t_i)] - \mathrm{Arg}[H_{kl}(t_0)] \tag{3}$$

which can take on values in the interval $[-\pi\ ;\ \pi\ [$. In Figs. 5(a) and 5(b) only curves for those fiber TM elements whose mean amplitude is larger than 0.18 are shown (27 out of 36 elements contained in the diagonal blocks), because of the higher relative noise on the remaining elements. It can be appreciated that the variations are quite small, the amplitude varying only within 25% of the mean and the phase only within $\pi/2$. From the fact that there are no large phase jumps, we conclude that the time resolution of our fiber TM measurement (40 min) is sufficient to resolve the slow drift under our experimental conditions. We further examine the time evolution of the fiber TM by computing the correlation coefficient between the first measured fiber TM at time t_0 with those measured at later times t_i. We define the correlation coefficient as:

$$C_{0i} = \frac{\sum_{k,l} H^*_{kl}(t_0) H_{kl}(t_i)}{\sqrt{\sum_{k,l} |H_{kl}(t_0)|^2}\ \sqrt{\sum_{k,l} |H_{kl}(t_i)|^2}} \tag{4}$$

where * denotes element-wise complex conjugation. The evolution of this correlation coefficient is presented in Fig. 5(c) (dots). The correlation coefficient remains above 70 % throughout which, again attests to the slow drift of the fiber TM. For reference, the temperature in close vicinity of the fiber was monitored during the measurements, it is shown in Fig. 5(d).

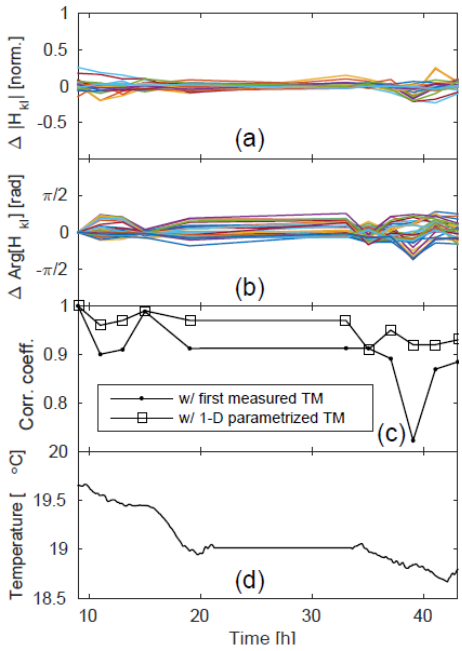

Figure 5. Temporal evolution of the fiber TM. (a) Normalized amplitude variation of fiber TM elements. (b) Phase variation of TM elements. Curves for fiber TM elements with negligible amplitude (< 0.18) are not shown. (c) Correlation coefficient between (dots) the first measured fiber TM and the ones measured at time t_i; (squares) the TM parametrized in one parameter and the fiber TM measured at time t_i. (d) Log of the temperature in the vicinity of the fiber during the measurement window.

An equivalent, but perhaps slightly more illustrative, representation of the same dataset is presented in Fig. 6. For each element, all 11 complex-valued fiber TM elements acquired at times t_i are plotted in the complex plane. Horizontal and vertical lines represent the real and imaginary axes, and the circles are guided to the eye with radius equal to the absolute value of the matrix element. This illustration allows us to observe that the drift in the fiber TM can be attributed mainly to a drift in the phase since all the 11 plotted points per sub-figure overwhelmingly tend to lie on the circles. However, this representation does not provide any insight on the correlation between the phase variations of the different elements, which is the topic of the next paragraph.

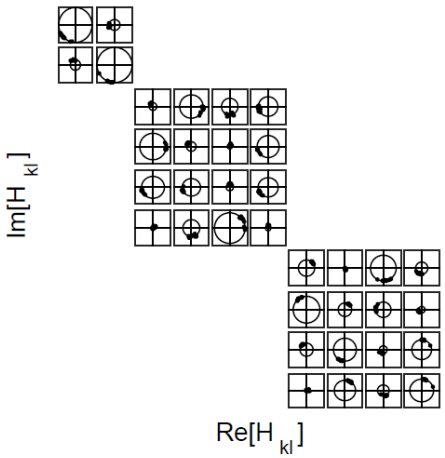

Figure 6. Representation in the complex plane of the fiber TM elements measured at different times. Horizontal and vertical lines represent the real and imaginary axes. Depicted circles are guides to the eye and have radius equal to the time-averaged norm of the fiber TM element.

Temporal evolution of the fiber TM

We will attempt to find a parametrization of the fiber TM that describes its temporal evolution. We start out from the stack of fiber TMs $H_{kl}(t_i)$ and the observation made in the previous paragraph that mainly the phase variation of the fiber TM needs to be considered. We create the two-dimensional matrix $\Delta\Phi_{\{kl\}i}$ in the composite index $\{kl\}$ and the temporal index i:

$$\Delta\Phi_{\{kl\}i} = \mathrm{Arg}[H_{kl}(t_i)] - \mathrm{Arg}[H_{kl}(t_0)], (k,l) \in D \tag{5}$$

Where D is the group of indices $(k,l)$of the diagonal blocks of the fiber TM. The matrix has dimension 36 x 11 (number of elements in the diagonal blocks x number of time points). We take the singular value decomposition of the resulting matrix (we omit the indices for brevity):

$$\Delta\Phi = U\,S\,V^{\dagger} \tag{6}$$

The first matrix U contains the left-singular vectors, S is a diagonal matrix formed by the singular values and V contains the right-singular vectors. We find a first singular value which is significantly larger than the rest. The first singular value accounts for 35% of the singular weight; the first three for 69%, and the first five for 88%. For now, we retain only the first singular vector which amounts to taking the first column of U, $U_{\{k,l\}1}$, with which we can construct an empirical, parametrized version of the fiber TM (in the parameter α):

$$H_{kl}^{(param)}(\alpha) = \begin{cases} H_{kl}(t_0)\,.\exp(j\alpha U_{\{kl\}1}), (k,l) \in D \\ H_{kl}(t_0) \qquad\qquad\qquad\quad , (k,l) \notin D \end{cases} \tag{7}$$

The drift is thus mathematically expressed as a complex-valued "drift" operator, identifiable as the matrix being multiplied onto $H_{kl}(t_0)$ in the Equation above. In Fig. 6, this drift operator is presented. We then checked whether the parametrized TM is a good model of the multi-modal channel represented by the fiber. To do so, for each fiber TM of the fiber TM stack we identify the α value that results in the largest inner product

$$C_i^{(param)} = \frac{\sum_{k,l}\left[H_{kl}^{(param)}(\alpha)\right] * H_{kl}(t_i)}{\sqrt{\sum_{k,l}\left|H_{kl}^{(param)}(\alpha)\right|^2}\ \sqrt{\sum_{k,l}|H_{kl}(t_i)|^2}} \tag{8}$$

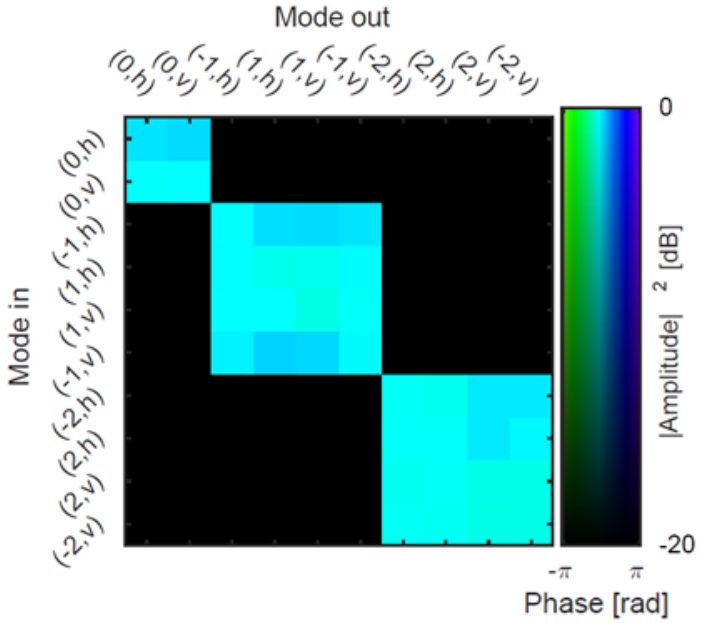

Figure 6. First singular vector of $\Delta\Phi$ in complex form-drift operator in the case of parametrization in one parameter.

The results are summarized in Tab. 3. It can be appreciated that this simple parametrization in only a single parameter gives a very decent description of the measured TMs with its 36 significant elements, with $C_i^{(param)}$ systematically above 0.9. The same values are also shown in Fig. 5(c) as squares.

Table 3. Correlation coefficient with the TM parametrized in one parameter.

$Time\ [h]$	α	$C_i^{(param)}$
9	0.00	1.00
11	1.54	0.96
13	1.49	0.97
15	0.17	0.99
19	1.48	0.97
33	1.18	0.97
35	-0.15	0.91
37	1.61	0.95
39	3.04	0.92
41	1.43	0.92
43	1.41	0.93

It is clear that parametrizing the TM in more parameters will result in ever better concordance with the measured fiber TMs. Nevertheless, we can conclude from our results that - in our measurement conditions - drift results in changes to the fiber TM that are highly correlated between matrix elements. Thus, even a low-dimensional parametrization with number of parameters much smaller than the number of matrix elements involved can describe the measurement very well.

4. DISCUSSION

The measurement of the full fiber TM is advantageous over indirect measurements like time-averaged cross-talk and bit-error ratio for allowing a direct measurement of the fiber's linear behavior and thus providing more information. As such, fiber TM measurements could be a good basis for developing empirical multi-modal channel models as well as for comparison with various multi-modal channel models that have been developed [19,20]. A fiber TM measurement resolved in wavelength, as was done in e.g. Ref. [17] would be required to elucidate also the group-delay effects for comparisons with models of group-delay behavior [21,22]. The length of the fiber studied here was very short, 1.5 m, but it is of the same length scale as some of the multi-mode components which would be required for potential future multi-modal fiber optic communication networks, like mode filters or few-mode amplifiers [23,24]. So, our method could be of interest for characterizing this type of multi-mode components. Fiber lengths that are pertinent for data transmission would of course be orders of magnitude longer. Knowing that the time scale of drift likely decreases as a function of length the fiber TM measurement would have to be made faster to retain its relevance for characterizing transmission fibers. The current time to measure a fiber TM, defining the temporal resolution, is 40 minutes. In principle this could be sped up in a number of ways that we have not yet implemented. We currently measure the four combinations of input and output polarizations separately, by measuring them simultaneously in a two-polarization setup an immediate gain of four would be achieved and, in addition, one would eliminate the source of error which is phase drift between measurements of different polarization combinations. Another way would be to reduce the number of local modes used in the initial measurement from the current 25x25 which is massively over-sampling the mode space of the fiber which guides only 10 vector modes; this would yield a proportional gain in measurement time. Finally, one could envision employing a SLM with shorter response time. Alternatively, we could measure directly in the basis of fiber modes, but this would preclude the ability to isolate the fiber TM from the misalignment.

5. CONCLUSION

We have described a method to measure the fiber TM of a ring-core FMF without misalignment contributions from the interfacing optics, and we have shown how a simple, low-dimensional parametrization of the fiber TM of a short length FMF gives a good insight about the temporal evolution of the multi-modal channel it represents over a time span of two days. We believe that our approach could help in developing accurate channel models for few-mode fiber optic transmission systems as well as getting a deeper understanding of FMFs.

ACKNOWLEDGMENTS

This work has been partially supported by the Agence Nationale de la Recherche through the LABEX CEMPI (ANR-11-LABX-0007) and the Equipex Flux (ANR-11-EQPX-0017), as well as by the Ministry of Higher Education and Research, Hauts de France council and European Regional Development Fund (ERDF) through the Contrat de Plan Etat-Region (CPER Photonics for Society P4S). FUI MODAL (FUI-AAP19).

REFERENCES

[1] P. P. Mitra and J. B. Stark, "Nonlinear limits to the information capacity of optical fiber communications," Nature 411, 1027-1030 (2001).
[2] P. J. Winzer, "Making spatial multiplexing a reality," Nat. Photon.8, 345-348 (2014).
[3] G. Li, N. Bai, N. Zhao, and C. Xia, "Space-division multiplexing: the next frontier in optical communication," Adv. Opt. Photon.6, 413-487 (2014).
[4] D. J. Richardson, J. M. Fini, and L. E. Nelson, "Space-division multiplexing in optical fibers," Nat. Photon. 7, 354-362 (2013).
[5] A. W. Snyder, "Coupled-mode theory for optical fibers," J. Opt. Soc. Am. 62, 1267-1277 (1972).
[6] A. Macho, M. Morant, and R. Llorente, "Experimental evaluation of nonlinear crosstalk in multi-core fiber," Opt. Express 23, 18712-18720 (2015).

[7] R. S. Luis, B. J. Puttnam, A. V. T. Cartaxo, W. Klaus, J. M. D. Mendinueta, Y. Awaji, N. Wada, T. Hayashi, and T. Sasaki, "Time and modulation frequency dependence of crosstalk in homogeneous multi-core fibers," J. Lightwave Technol. 34, 441-447 (2016).
[8] G. Rademacher, R. S. Luis, B. J. Puttnam, Y. Awaji, and N.Wada, "Performance fluctuation in direct detection multi-core fiber transmission systems," in ECOC (2017) pp. Poster Session II: SC 6 – Point-to-Point Transmission Links.
[9] B. J. Puttnam, G. Rademacher, R. S. Luis, W. Klaus, Y. Awaji, and N. Wade, "Inter-core crosstalk spectrum and penalty measurements in 7-core fiber," in ECOC (2017).
[10] T. M. F. Alves, R. S. Luis, B. J. Puttnam, A. V. T. Cartaxi, Y. Awaji, and N. Wada, "Performance of adaptive dd-ofdm multicore fiber links and its relation with intercore crosstalk," Opt. Express 25, 16017-16027 (2017).
[11] T. M. F. Alves and A. V. T. Cartaxo, "Intercore crosstalk in homogeneous multicore fibers: theoretical characterization of stochastic time evolution," J. Lightwave Technol. 35, 4613-4623 (2017).
[12] T. M. F. Alves and A. V. T. Cartaxo, "Characterization of icxt in dd-ofdm mcf-based systems," in ECOC (2017).
[13] L. Gan, L. Shen, T. M., C. Xing, Y. Li, C. Ke, W. Tong, B. Li, S. Fu, and D. Liu, "Investigation of channel model for weakly coupled multicore fiber," Opt. Express 26, 5182-5199 (2018).
[14] T. M. F. Alves and A. V. T. Cartaxo, "Characterization of the stochastic time evolution of short-term average intercore crosstalk in multicore fibers with multiple interfereing cores," Opt. Express 26, 4605-4620 (2018).
[15] N. Bozinovic, Y. Yue, Y. Ren, M. Tur, P. Kristensen, H. Huang, A. E. Willner, and S. Ramachandran, "Terabit-scale orbital angular
momentum mode division multiplexing in fibers," Science 340, 1545-1549 (2013).
[16] M. Plöschner, T. Tyc, and T. Cizmar, "Seeing through chaos in multimode fibers," Nat. Photon. 9, 529-535 (2015).
[17] J. Carpenter, B. J. Eggleton, and J. Schröder, "Observation of Eisenbud-Wigner-Smith states as principal modes in multimode fiber," Nat. Photon. 9, 751-757 (2015).
[18] E. Cuche, P. Marquet, and C. Depeursinge, "Spatial filtering for zero-order and twin-image elimination in digital off-axis holography," Appl. Opt. 39, 4070-4075 (2000).
[19] C. Antonelli, A. Mecozzi, M. Shtaif, and P. Winzer, "Random coupling between groups of degenerate fiber modes in mode multiplexed transmission," Opt. Express 21, 9484-9490 (2013).
[20] K. P. Ho and J. M. Kahn, "Mode-dependent loss and gain: Statistics and effect on mode division multiplexing," Opt. Express 19, 16612-16635 (2011).
[21] K. P. Ho and J. M. Kahn, "Statistics of group delays in multimode fiber with strong mode coupling," J. Lightwave Technol. 29, 3119-3128 (2011).
[22] K. P. Ho and J. M. Kahn, "Delay-spread distribution for multimode fiber with strong mode coupling," IEEE Photon. Technol. Lett. 24, 1906-1909 (2012).
[23] J.-B. Trinel, Y. Quiquempois, A. Le Rouge, G. Le Cocq, L. Garcia, J.-F. Morizur, G. Labroille, and L. Bigot, "Amplification sharing of non-degenerate modes in an elliptical-core few-mode erbium-doped fiber," Opt. Express 24, 4654-4661 (2016).
[24] J.-B. Trinel, G. Le Cocq, E. R. Andresen, Y. Quiquempois, and L. Bigot, "Latest results and future perspectives on few-mode erbium doped fiber amplifiers," Opt. Fiber Technol. 35, 56-63 (2016).
[25] M. Born and E. Wolf, Principles of Optics (Cambridge, 1999).